Interpretation of Synchrotron Radiation Circular Dichroism Spectra of Anionic, Cationic, and Zwitterionic Dialanine Forms

Jiří Šebek,[†,‡] Bela Gyurcsik,[§] Jaroslav Šebestík,[†] Zdeněk Kejík,[‡] Lucie Bednárová,[†] and Petr Bouř*[,†]

Institute of Organic Chemistry and Biochemistry, Academy of Sciences of the Czech Republic, Flemingovo nám. 2, 166 10, Prague 6, Czech Republic, Department of Analytical Chemistry, Institute of Chemical Technology, Technická 5, 166 28, Prague 6, Czech Republic, and Department of Inorganic and Analytical Chemistry, University of Szeged, P.O. Box 440, H-6701 Szeged, Hungary

Received: December 21, 2006; In Final Form: February 7, 2007

Electronic absorption and synchrotron radiation circular dichroism (SRCD) spectra of the anionic, cationic, and zwitterionic forms of L-alanyl-L-alanine (AA) in aqueous solutions were measured and interpreted by molecular dynamics (MD) and ab initio computations. Time-dependent density functional theory (TD DFT) was applied to predict the electronic excited states. The modeling enabled the assessment of the role of molecular conformation, charge, and interaction with the polar environment in the formation of the spectral shapes. Particularly, inclusion of explicit solvent molecules in the computations appeared to be imperative because of the participation of water orbitals in the amide electronic structure. Implicit dielectric continuum solvent models gave inferior results for clusters, especially at low-energy transitions. Because of the dispersion of transition energies, tens of water/AA clusters had to be averaged in order to obtain reasonable spectral shapes with a more realistic inhomogeneous broadening. The modeling explained most of the observed differences, as the anionic and zwitterionic SRCD spectra were similar and significantly different from the cationic spectrum. The greatest deviation between the experimental and theoretical curves observed for the lowest-energy negative anion signal can be explained by the limited precision of the TD DFT method, but also by the complex dynamics of the amine group. The results also indicate that differences in the experimental spectral shapes do not directly correlate with the peptide main-chain conformation. Future peptide and protein conformational studies based on circular dichroic spectroscopy can be reliable only if such effects of molecular dynamics, solvent structure, and polar solvent−solute interactions are taken into account.

Introduction

Electronic circular dichroism (often referred to as CD, ECD, or UV CD) spectroscopy, monitoring the difference in absorption of left and right circularly polarized light, has been used for molecular conformational studies for a long time.[1] More recently, synchrotron radiation CD has emerged as a technique that provides higher signal-to-noise ratios and enables measurements at lower wavelengths than classical spectrometers equipped with xenon arc lamps.[2] Because dichroism is usually more sensitive to the molecular shape than single absorption, this technique has helped to elucidate many questions associated with the structures and dynamics of saccharides,[3,4] proteins,[5−8] and nucleic acids.[9,10] Although the interpretation has traditionally been based rather on empirical experience,[1,11−15] the latest advances in time-dependent density functional theory (TD DFT)[16−19] have made it possible to predict properties of excited electronic states for large systems that could not be tackled with classical wavefunction-based methods.[20−23] Considerable progress has also been achieved in terms of understanding the amide chromophore electronic structure and its interaction with the environment.[13,22,24−31]

However, it was quickly recognized that environmental factors, which play a comparatively minor role in vibrational spectroscopy,[32,33] are instrumental in understanding electronic spectra obtained in solutions.[22,27,34−37] Apart from the undisputed dependence on peptide conformation, the electronic transition energies are also modulated by the special distribution of the solvent (water) molecules, via their electrostatic field and a direct involvement of the solvent electronic structure.[27,35,38,39] Coupling of vibrational motion with the electronic transition energies and intensities also contributes to the peptide spectral shapes, but probably less so than the conformation and the solvent.[27]

Because of the complexity of electronic phenomena, it is important to assess the relative impacts of all of the factors affecting the spectra and identify the processes involved, with the aim of relating structures and dynamics to experimentally detectable values. This is also the chief reason why we assess the performance of available simulation techniques as applied to the absorption and ECD spectra of L-alanyl-L-alanine (AA). For AA, the anionic, cationic, and zwitterionic forms of the molecule can easily be induced by pH variation.[40,41] Similarly, a significant pH dependence of the ECD spectra of trialanine (AAA) was observed.[42] The AA molecule shares many important properties with longer biopolymers and is widely used in benchmark and testing computations.[43−50] Although some conceptual problems have been reported for the application of DFT to electron-transfer phenomena,[51,52] we use the B3LYP

* To whom correspondence should be addressed. E-mail: bour@uochb.cas.cz.
† Academy of Sciences of the Czech Republic.
‡ Institute of Chemical Technology.
§ University of Szeged.

10.1021/jp068811y CCC: $37.00
Published on Web 03/17/2007

DFT functional that has been, at least on an empirical basis, found acceptable for the semiquantitative prediction of the electronic spectra of a large ensemble of systems.[36,50,53] We also performed trial computations with three other common functionals, which, however, did not provide convincingly better results within the entire spectral range. Among all of the factors influencing CD spectra, solvent averaging appears to be the most complex task. The present study also indicates that the participation of the water electronic structure in the amide group transitions is essential for the interpretation of spectra of longer peptides and proteins.

Methods

The AA peptide was prepared according to the procedure described elsewhere.[54] The synchrotron radiation CD (SRCD) spectra of various AA forms were recorded at the SRCD facility at the UV1 beamline,[55] itself part of the ASTRID storage ring at the Institute for Storage Ring Facilities (ISA), University of Aarhus, Aarhus, Denmark. The light passed from the synchrotron (linear polarization) through a CaF_2 window into a CD instrument purged constantly with nitrogen. The polarization was converted into an alternating circularly polarized light. A CaF_2 photoelastic modulator (PEM, model I/CF50, Hinds Instruments, Hillsboro, OR) operating at 50 kHz was used. The signal was detected with a photomultiplier tube (PMT, 9402B, Electron Tubes, Ruislip, U.K.) fitted with a lock-in amplifier. Camphor−sulfonic acid was used to calibrate the instrument. All spectra were recorded in 1-nm steps with a dwell time of 3 s per step, in 18- and 6-μm quartz cells (SUPRASIL, Hellma GmbH, Müllheim, Germany), in the wavelength ranges of 178−350 and 168−350 nm, respectively. The peptide was dissolved in distilled water (final AA concentration of 25 mmol/dm^3), and the solution pH was adjusted with HCl and NaOH solutions; the water baseline was subtracted from the raw CD spectra. Absorption spectra were measured with a Pye Unicam PU8800 spectrometer in a 0.2-mm cell (final AA concentration of 7.6 mmol/dm^3). Both of the available measurement modes were applied: (1) direct reading of absorbance against deionized water and (2) differential reading against HCl or NaOH solution. Control recordings of CD and absorption spectra were performed on other spectrometers (data not shown).

Spectra were simulated by a time-dependent DFT calculation[17] using the B3LYP[56] functional and the 6-311++G** Pople-type basis set, as implemented in the Gaussian programs.[57] For AA/water clusters, a combination of the 6-311++G** and 6-31G basis sets had to be used to obtain results in reasonable time. As illustrated in Figure 1, the larger basis set was used for the amide group atoms and also for the carboxyl group. These two moieties are expected to contribute primarily to the lowest-energy AA absorption and CD bands. The aqueous environment was modeled with the Gaussian implementation of the COSMO model, also referred to as CPCM.[58] Trial computations were performed with the PCM solvent model[59] and BHLYP,[56,60] BPW91,[56] and HCTH[61] DFT functionals.

For an alternative solvent model, AA/water clusters were generated with the TINKER molecular dynamics package.[62] The AA molecules were placed in a cubic periodic water box 18.62 Å wide. The Amber94 peptide force field,[63] TIP3P water model,[64] and an *NpT* ensemble were applied at the temperature of 300 K and pressure of 1 atm. The force field was appended by additional constraints on the main-chain torsion angles in AA, based on the presumably more accurate BPW91/PCM/6-311++G** potential energy surfaces[54] with equilibrium angle values listed in Table 1. After minimization and a 100-ps equilibrium phase, geometries were recorded every 10 ps. Sets of 100 configurations were obtained for each of the three charged forms, AA^+ (cation), AA^- (anion), and $AA^\pm$ (AAZW, zwitterion). For AA^-, two conformers were explored, and additional constraints on the rotation of the CO_2^- and NH_2 groups were applied to detect the effects of these motions on the spectra. From the MD geometries, AA/water clusters were selected so that only hydrogen-bonded water molecules closer than 2.2 Å to the peptide were retained, which resulted in systems with 4−9 water molecules. These systems were then subjected to ab initio computations in Gaussian. Five optimization steps were run first to correct the greatest inaccuracies of the Amber force field, and the absorption and CD spectra were then calculated by the TD DFT method. As follows from test computations [Figure 1s in the Supporting Information (SI)], this seemingly primitive procedure appears quite appropriate for the given purpose, as the high-frequency vibrational degrees of freedom (normal modes) quickly relax (within 1−3 steps) and then the electronic spectral pattern is for some time (~10 steps) reasonably stabilized until the water molecules start to translate and rotate.

The explicit clusters were treated with and without the CPCM correction for the remaining solvent. The absorption and CD spectra were generated from the calculated dipole and rotational strengths using Lorentzian bands with a full width at half-height (fwhh) of 5 nm. To analyze the amide electronic structure in a large ensemble of molecules and clusters, electronic transitions were assigned with the aid of our programs[27] that explore the excited electronic states on the basis of overlaps $S_{IJ} = |\langle\bar{\Psi}_I|\Psi_J\rangle|$ between the $\bar{\Psi}_I$ and Ψ_J molecular orbitals in a

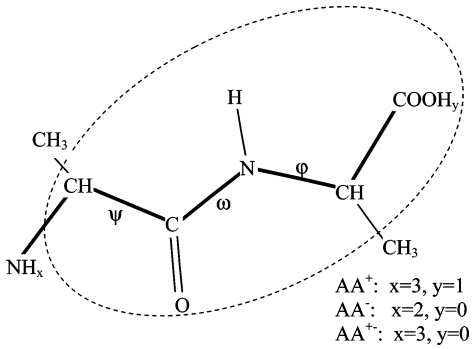

Figure 1. Main-chain torsion angles in the three Ala−Ala forms. For atoms within the dashed ellipse, the 6-311++G** basis was used in the ab initio cluster computations, whereas for the rest of the molecule and explicit water molecules in the clusters, the smaller 6-31G basis was applied. For computations without explicit water molecules, the 6-311++G** basis was used for all atoms.

TABLE 1: Calculated Equilibrium Geometries of the AA Forms

	φ	ψ	ω
BPW91/CPCM/6-311++G**			
AA^+	−141	150	175
AAZW	−156	149	172
$AA^-(1)^a$	−153	134	175
$AA^-(2)$	−151	−20	179
B3LYP/CPCM/6-311++G**			
AA^+	−143	151	175
AAZW	−156	149	173
$AA^-(1)^b$	−154	133	175
$AA^-(2)$	−154	−19	179
BPW91/PCM/6-311++G**			
AAZW[c]	−153	147	173

[a, b] Relative conformer energies (of 1 with respect to 2) of 0.3 and 0.5 kcal/mol, respectively. [c] Reference 54.

TABLE 2: Average AA Torsion Angles and Their RMS Deviations (Δ, in deg) Obtained by the Molecular Dynamics Simulation with Explicit Solvent

	φ^a	ψ^a	$\Delta\varphi$	$\Delta\psi$
AA^+	−117	147	5.5	5.5
AAZW	−145	147	5.3	5.1
$AA^-(1)$	−148	125	5.2	5.8
$AA^-(2)$	−150	−21	4.6	5.5
$AA^-(1)^b$	−149	120	5.1	5.3
$AA^-(2)^b$	−150	−20	4.3	6.0

[a] Angles φ and ψ were partially restrained to the values obtained at the BPW91/CPCM/6-311++G** level (Table 1) via a harmonic penalty function with a barrier of 0.01 kcal/mol/deg[62] [b] Additionally, the NH_2 and CO_2^- rotations were fixed according to the BPW91/CPCM/6-311++G** equilibrium geometries. Average H−N−C−C torsion angles (and deviations) were 168(3)° and 58(7)° and average N−C−C=O angles were −18(4)° and −55(7)° for 1′ and 2′, respectively.

reference system (NMA) and the actual system (AA), respectively. Various computer resources were involved, including Linux-based PCs and supercomputers. For example, one cluster optimization (from the total number of 500) took typically about 1.5 h and a spectrum computation took about 4.5 h on three IA-64 1.3-GHz processors with 2 GB of memory.

Results and Discussion

Geometry. In all of the AA forms, the rotation of the main-chain torsion angles (φ, ψ; Figure 1) is limited, and the DFT methods provide well-defined global minima, as summarized in Table 1. A systematic conformer search predicted that other local minima were also possible for $AA^\pm$ and A^+, but were not significantly populated at room temperature. For AA^-, two conformers (1, 2) were predicted with energies within ~0.5 kcal/mol according to the various approximations (PCM, CPCM, B3LYP, BPW91) employed. The BPW91 and B3LYP functionals provided similar potential energy surfaces. A more detailed analysis of the AA^+ potential (not shown) indicates that the minimum is quite shallow and the φ angle can vary within the range from approximately −102° to −143°. Otherwise, the three conformers, AA^+, AAZW, and $AA^-(1)$, appear to be rather similar, with AA^+ and AAZW differing more in φ whereas AAZW and AA^- differ more in ψ. The differences thus nicely reflect the change of the molecular charge: the angle φ can be controlled by a change in charge at the carboxyl group, whereas the angle ψ is more sensitive to amine group protonation. The lowest-energy conformations of $AA^\pm$, AA^+, and $AA^-(1)$ are similar to the polyproline II type recently proposed for alanine-containing peptides on the basis of CD temperature dependence.[31] However, in AA^-, we can see that the other form (2) is energetically favorable, and it will also provide spectra that more closely match the experimental data. This form is stabilized by an intramolecular hydrogen bond between the nitrogen of the $-NH_2$ group and the amide hydrogen, with the participation of the nonbonded N electron pair. In contrast, in structure 1, it is the amine ($-NH_2$) hydrogen that forms a hydrogen bond with the amide oxygen.

Average angle values and RMS deviations in sets of 100 clusters used for spectral calculations are summarized in Table 2. The averages are mostly close to the equilibrium values in Table 1, as desired. This match was achieved through the adaptation of the Amber force field; the somewhat different central value of the angle φ in AA^+ corresponds to the shallow potential profile of this rotation. The RMS deviations given in Table 2 reflect the Boltzmann distribution obtained by analyses of full potential energy surfaces (ref 54 and unpublished results).

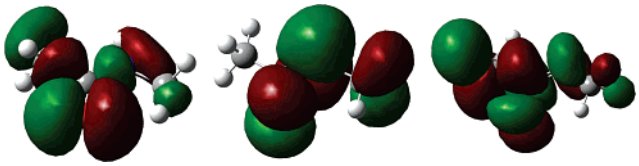

Figure 2. *n*, π, and π^* (from left to right) B3LYP/6-311++G** orbitals of *N*-methylacetamide.

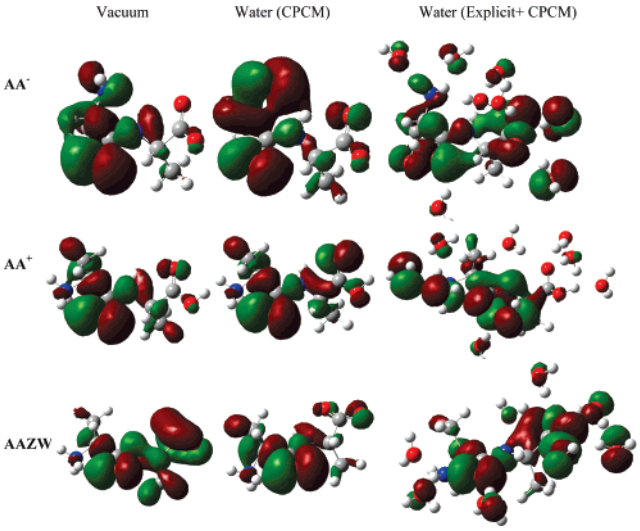

Figure 3. Nonbonded (*n*) amide oxygen orbital in the three dialanine forms calculated (B3LYP/6-311++G**) in a vacuum, with the continuum and explicit solvent models. The dipeptide is kept in similar orientations in the plots.

For the two AA^- conformers of distinct (φ, ψ) angles, additional sets of clusters were constructed, as listed in the last two rows in Table 2, where additional restrictions were applied to the $-NH_2$ and CO_2^- group rotations. As discussed earlier,[54,65] continuum polarization solvent models might not be adequate for the description of the strong directional hydrogen bonds of the polar groups, and it is difficult to select the best description of the dynamics with the applicable computational means. Thus, we used the restriction based on the PCM models as an alternative to the Amber empirical force field. The latter model leads to a greater flexibility of the $-NH_2$ and CO_2^- groups as they frequently form hydrogen bonds with solvent molecules.

Amide Electronic Structure. To classify the AA electronic structure and separate the amide contributions from those of the other molecular parts and the solvent, calculated molecular orbitals were overlapped and compared with those obtained for *N*-methylacetamide (NMA). The *n*, π, and π^* orbitals found to be the most important for peptide and protein CD[10] are plotted for NMA in Figure 2. The *n* orbital can be regarded as the free oxygen electron pair within the amide plane, although it is also delocalized over the rest of the NMA molecule. The π and π^* orbitals are antisymmetric with respect to the amide plane. As is apparent from Figures 3−5, these orbitals can also be identified in the AA forms. However, a closer inspection reveals several changes already in a vacuum. Among the three orbitals shown, the π^* orbital (Figure 5) appears to differ most in the AA forms when compared to NMA. The vacuum orbital shapes are further altered when the PCM solvent correction is applied. The solvent, similarly to when the protonation changes, induces considerable changes in the π^* orbital. However, even in the *n* and π orbitals, differences between the vacuum and PCM models are apparent for the zwitterion, whereas the other two forms do not differ that much. This might be related to the

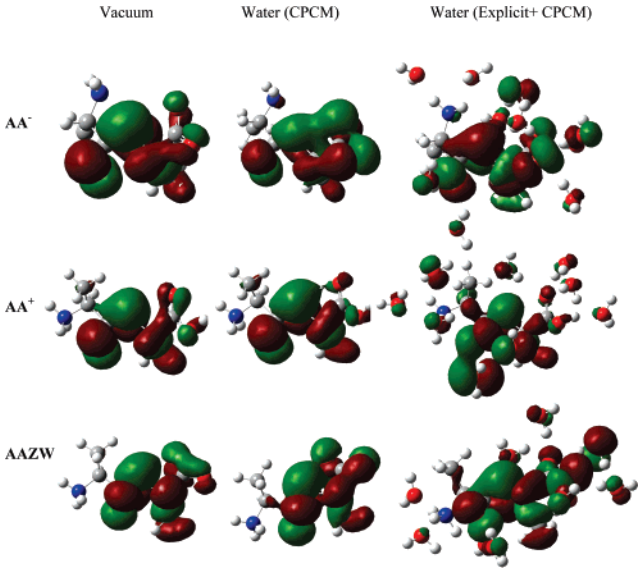

Figure 4. π amide orbital in the three dialanine forms obtained (B3LYP/6-311++G**) for a vacuum, with the continuum and explicit solvent models.

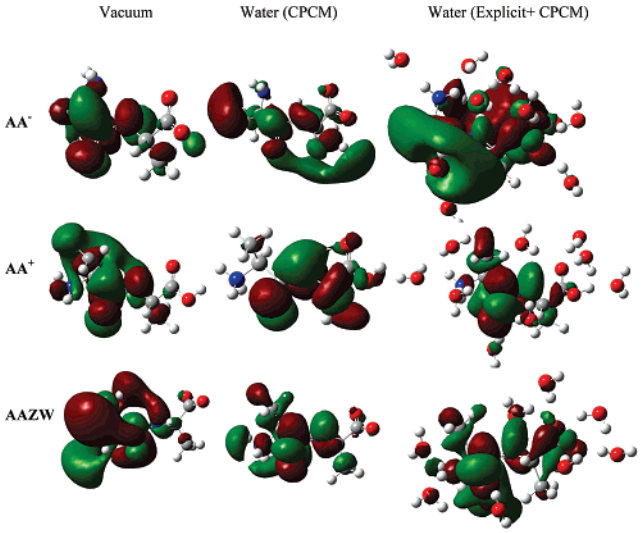

Figure 5. Antibonding π^* orbital in the AA forms obtained by B3LYP/6-311++G** in a vacuum, with the continuum and explicit solvent models.

instability of AAZW in vacuum. For the explicit water cluster (selected randomly from the MD run and shown on the right-hand side in Figures 3−5), the orbitals are also distorted compared to vacuum. Moreover, the hydrogen-bonded water molecules directly participate in the orbital structure as previously observed for NMA.[27] The π^* orbitals of the AA^- form even resemble a delocalized "Rydberg-type" orbital comprising many solvent molecules. Even in NMA, the $\pi^{*\prime}$ amide orbital is significantly mixed with delocalized contributions from more distant molecular parts. The basis set limitation in the mixed 6-311++G**(6-31G) scheme does not seem to be a significant limitation for the description of the occupied and amide-centered virtual orbitals (examples of n, π, and π^* orbitals obtained with the mixed and full 6-311++G** basis can be found in Figure 2s in the SI). Obviously, the current basis might not be sufficient for higher-energy and true Rydberg electronic states.

Electronic Transitions. The changes in the electronic structure are reflected in the transition energies and dipole strengths summarized in Tables 3 and 4, respectively. Most

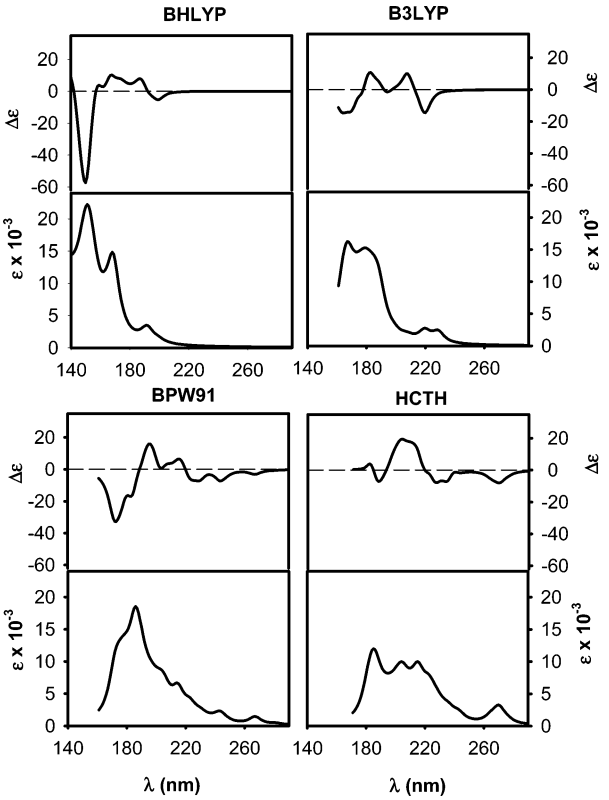

Figure 6. Computed [6-311++G**(6-31G)/CPCM] absorption and CD spectra for an arbitrarily selected AA^-/water cluster with the BHLYP, BPW91, B3LYP, and HCTH functionals.

transitions observed in NMA could also be identified in the dipeptide. However, it is essential to realize that the assignment based on the best orbital overlaps is mechanistic and does not have any physical consequences. Especially the vacuum orbitals of AAZW differed significantly from the NMA reference, and transition number 3 in the vacuum model could not be assigned at all. This reflects the instability of the zwitterionic form in a vacuum, much like the volatility of its orbitals mentioned above. Different NMA transitions (4 and 6) were assigned to the same AAZW bands; multiple assignments occurred for AA^- as well. In spite of all of these minor discrepancies, however, we can see that the NMA amide chromophore mostly preserves its electronic structure in the dipeptide forms. Similar amide locality has been assumed in peptide and protein spectroscopy for a long time, in light of the experimental evidence.[10] Each transition varies to a very different extent with the molecular charge and environment. For example, the first $n-\pi^*$ AA^- transition is lower in wavelength with CPCM (189 nm) than in a vacuum (206 nm), whereas the opposite order is observed for AA^+ and AAZW. For the CPCM computations, the lowest-energy (highest-wavelength) transitions appear to be the most sensitive to changes in the amide group environment.

Much larger changes can be observed for the dipole strengths listed in Table 4. Even for the energetically close transitions, the strengths often differ by a factor of 2 and more. This can be explained by the coupling of the amide orbitals with the whole AA electronic structure, as well as by polarization caused by the AA charged residues. Transition coupling and intensity distribution among the transitions would also explain the rather similar sums of the dipole strengths (last row in Table 4). Interestingly, both the vacuum and CPCM models predict the absorption to be approximately inversely proportional to the number of protons in the AA molecule.

TABLE 3: Ten Lowest-Energy Amide Transition Wavelengths (in nm) in NMA and the AA Forms as Calculated at the B3LYP/6-311++G Level**

	vacuum				CPCM			
transition	NMA	AA^+	AAZW	$AA^-(2)$	NMA	AA^+	AAZW	$AA^-(2)$
1 $n-\pi^*$	217	203	170	206	206	211	203	189
2	216	164	169	264	201	184	187	191
3	214	158	—[a]	267	191	178	184	186
4	191	146	240	267	173	165	163	189
5	190	153	296	264	182	170	170	181
6	183	208	240	267	168	162	165	175
7	181	216	296	264	175	166	170	174
8 $\pi-\pi^*$	176	186	194	178	179	181	180	181
9	175	135	190	235	162	161	165	177
10 $\pi-\pi^*$	175	140	160	231	168	164	166	170

[a] Analogous transition not found.

TABLE 4: Calculated NMA and AA Amide Dipole Strengths (in Debye,[2] for the Transition Energies in Table 3)

	vacuum				CPCM			
transition	NMA	AA^+	AAZW	AA^- (2)	NMA	AA^+	AAZW	AA^- (2)
1 $n-\pi^*$	0.03	0.03	0.60	0.12	0.03	0.11	0.83	0.09
2	0.00	0.34	0.20	0.12	0.07	0.78	1.13	0.37
3	0.55	0.84	—	0.37	0.85	2.24	0.83	0.26
4	0.57	0.33	0.02	0.42	0.63	0.26	0.56	0.09
5	0.38	0.32	0.07	1.31	0.34	0.35	0.50	0.13
6	0.56	0.93	0.02	0.37	1.40	0.50	0.91	0.65
7	0.28	0.05	0.07	0.12	0.40	0.95	0.31	1.84
8 $\pi-\pi^*$	3.50	5.18	1.53	0.11	10.46	8.14	4.17	0.13
9	0.00	0.29	0.61	0.05	0.01	0.29	0.06	0.52
10 $\pi-\pi^*$	2.53	0.25	0.61	0.11	0.73	0.54	0.65	0.45
sum	8.40	8.56	3.73	3.10	14.92	14.16	9.95	4.53

TABLE 5: Calculated (B3LYP/CPCM/6-311++G) Energies (nm)[a] of Low-Energy Carboxyl Transitions**

transition	AA^+(COOH)	AAZW (COO^-)	AA^- (COO^-)
1 $n_{COO}-\pi^{*\prime}$	211 (0.002)	216 (0.001)	214 (0.009)
2 $n_{COO}-\pi^*$	209 (0.003)	220 (0.010)	219 (0.020)
3 $\pi_{COO}-\pi^*$	161 (0.015)	197 (0.013)	199 (0.013)
4 $\pi-\pi^*_{COOH}$	184 (0.211)	—	—

[a] Oscillator strengths in parentheses.

Experimental ECD studies revealed an important contribution of the carboxyl group to the UV and ECD spectra of short peptides.[41] Calculated energies and oscillator strengths of these transitions are reported in Table 5 for the CPCM model. The computation indicates distinct spectral changes between the protonated and negative forms, in accord with the experimental observations. The negative group starts to absorb at lower wavelengths (214−216 cm^{-1}) than the protonated form (211 cm^{-1}) because of the $n_{COO}-\pi^{*\prime}$ transition. The "$\pi^{*\prime}$" orbital comprises the amide π system and delocalized space around the NH_n/CH_3 groups. However, the frequency difference is relatively minor, and the oscillator strengths are small. The n_{COO} orbital shapes (not shown) in the COO^- and COOH groups are very similar. Therefore, as suggested before,[41] the $n_{COO}-\pi^*$ transition causes greater changes. Indeed, for the deprotonated forms (AAZW, AA^-), the absorption wavelength of this transition rises by about 10 nm compared to that of AA^+, and the oscillator strength more than doubles. Finally, the $\pi_{COO}-\pi^*$ transition is predicted to contribute to the AAZW and AA^- spectra around 197−199 nm, although its wavelength is probably too low to be separately detectable for AA^+; for the latter form, a new low-energy $\pi-\pi^*_{COO}$ transition is predicted at 184 nm. The results suggest that the B3LYP method can reasonably well describe charge-transfer transitions, at least between close chromophores. However, it is difficult to separate the COO^-/COOH transitions from those of the amide and other molecular parts because of the electron delocalization. The absorption intensity of the amide transitions is stronger and contributes more to the AA ECD spectra.

The results also confirm previous findings indicating the necessity to include explicit water molecules for faithful simulation of aqueous solution spectra.[20] The averaging over many MD configurations makes the computations difficult and restricts them currently to DFT methods. On smaller systems, higher-level wavefunction (CC) computations occasionally provide better agreement with experiment,[20] and the limited accuracy of TD DFT can potentially account for part of the error in the simulated spectra, specifically, in the high-frequency region.[38] On the other hand, we did not observe a significant drawback for TD DFT compared to MRCI or CASPT2 for *N*-methylacetamide.[27] Generally, the DFT functionals are rarely optimized to reproduce excited electronic state properties;[52,66] this problem, however, lies beyond the scope of the present work.

In Figure 6, we compare absorption and CD spectra computed with four different functionals, i.e., BHLYP,[67] B3LYP,[68] BPW91,[69] and HCTH,[70] for an AA^-/water cluster. The basic characteristics of the spectra seem to be similar in all cases, that is, a weaker absorption and a negative CD at the longest wavelengths (CD minima at 197, 220, 270, and 271 nm, respectively, for the four functionals), whereas for short wavelengths, the absorption achieves its maximum (at about 152, 165, 187, and 185 nm, respectively), perhaps accompanied by a negatively biased −/+ CD couplet. Except for these similarities, the four functionals lead to very different frequency and relative intensity distributions. It is also difficult to trace individual electronic transitions across various DFT levels, because the orbital shapes are very different. Without more abstract guidelines, we, as many others, opted for the B3LYP functional, as it provides electronic transition energies reasonably close to the experimental values.[36,66] Similar results can also

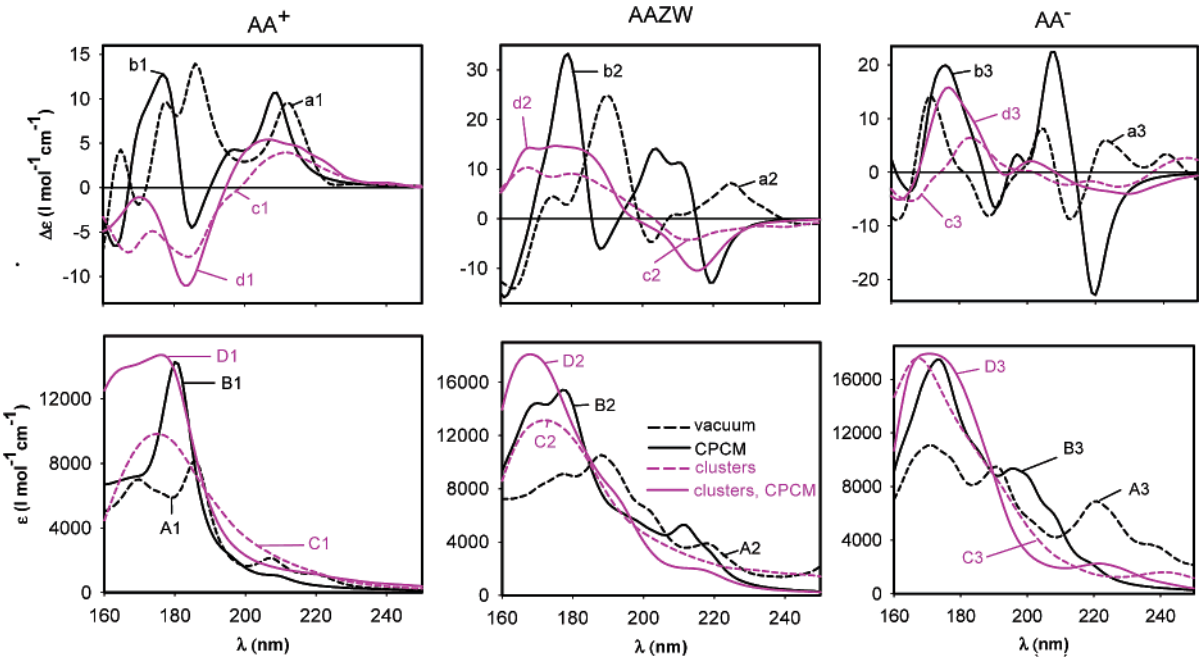

Figure 7. CD (top) and absorption (bottom) spectra of AA^+, AAZW, and AA^-, simulated with different solvent models: vacuum (dashed black lines, traces a1−3, A1−3), CPCM dielectric model (solid black lines, b1−3, B1−3), and average over 100 explicit clusters with hydrogen-bonded water molecules from the first hydration sphere in a vacuum (dashed magenta, traces c1−3, C1−3) and with the CPCM (solid magenta, d1−3, D1−3).

be obtained for other clusters or the AAZW and AA^+ ions. Among the four functionals, BPW91 and HCTH appear to be most problematic for faithful modeling, as they often provide unrealistically high (up to 900 nm) absorption thresholds, albeit accompanied by low absorption. The BHLYP functional leads to better agreement with experiment for higher wavelengths (∼210 nm) than does B3LYP; however, the BHLYP $\pi-\pi^*$ absorption maximum (at ∼152 nm) is unrealistically low.

Solvent Modeling. The performance of explicit and implicit solvent models is compared in Figure 7, where AA^-, AA^+, and AAZW CD and absorption spectra are simulated in a vacuum, with continuum and cluster solvent, as well as a combination of clusters and the continuum. Clearly, the spectra are very sensitive to the environment of the peptide. Compared to vacuum (dashed lines), the CPCM continuum (solid lines) leads to an overall increase of the absorption intensity and a shift of the absorption threshold to lower wavelengths, by ∼5−20 nm. However, individual low-intensity transitions (not visible in the figure) appear up to ∼900 nm for the vacuum computations. The vacuum approximation is thus clearly inappropriate for simulations of the electronic properties. Addition of the explicit solvent (spectra C1−3) has an effect similar to that of the CPCM continuum (B1−3), in terms of qualitative changes in the spectra, namely, an average intensity increase and a leftward shift of the absorption threshold compared to vacuum (A1−3). However, further addition of the CPCM continuum (D1−3) still significantly modifies the spectra, specifically, increasing absorption in the lower-wavelength region. These differences are emphasized in CD: plain vacuum AA spectra (a1−3) appear quite unsuitable for reproduction of the solution signal, as they often exhibit a sign opposite to that obtained with the continuum solvent added (b1−3). One might argue that the basic sign pattern, especially for the shortest-wavelength regions of AA^-, is already apparent in a vacuum; nevertheless the solvent clearly changes the analytically most important longer-wavelength regions. The addition of hydrogen-bonded water molecules (c1−3, d1−3) changes the intensity still more, to the same extent as the implicit solvent, namely, in the highest-wavelength region (∼200−250 nm). Inclusion of the explicit solvent thus appears imperative for correct modeling, as has also been found for similar polar systems.[27,35,39] On the other hand, addition of the polarizable continuum to the explicit clusters (cf. sets c1−3 and d1−3) causes relatively small changes, and the theoretical CD shapes start to converge. Thus, we can expect that the first hydrogen-bond hydration water shell represents most of the solvent interactions as they appear in the spectra.

Not only are the average amide transition energies and intensities affected by the inclusion of the implicit solvent, but the spectra are significantly influenced by the momentary solvent distribution. This can be demonstrated in Figure 8, where transition wavelengths of the 10 lowest-energy amide transitions are plotted for 100 AA^-/water clusters. In the lower part of the figure, the dependence of the wavelengths on the C═O bond length is extracted for the $n-\pi^*$ and $\pi-\pi^*$ transitions. Similarly to *N*-methylacetamide[27] or DNA chromophores,[37] various transitions are differently sensitive to the solvent configuration, which implies the need to average a great number of geometries to obtain realistic inhomogeneous band widths. No clear relation is visible between the transition energies and the C═O bond lengths, probably because of the complicated solvent−solute interactions, including purely electrostatic terms as well as a charge transfer.[27]

Calculation versus Experimental Spectra. The experimental absorption and SRCD data for the three AA forms are compared with the averaged cluster spectra in Figure 9. In general, the experimental CD and absorption intensity changes caused by varying pH agree with previous observations.[41] Most notably, the zwitterionic form exhibits the strongest absorption and starts to absorb at higher wavelengths than the positively and negatively charged forms. At short wavelengths, the negative form absorbs significantly less than the other two. It is important to note that the signal of the pH-adjusting agents (HCl, NaOH) had to be carefully subtracted because of their strong absorption at lowest wavelengths. Even with this subtraction, however, the

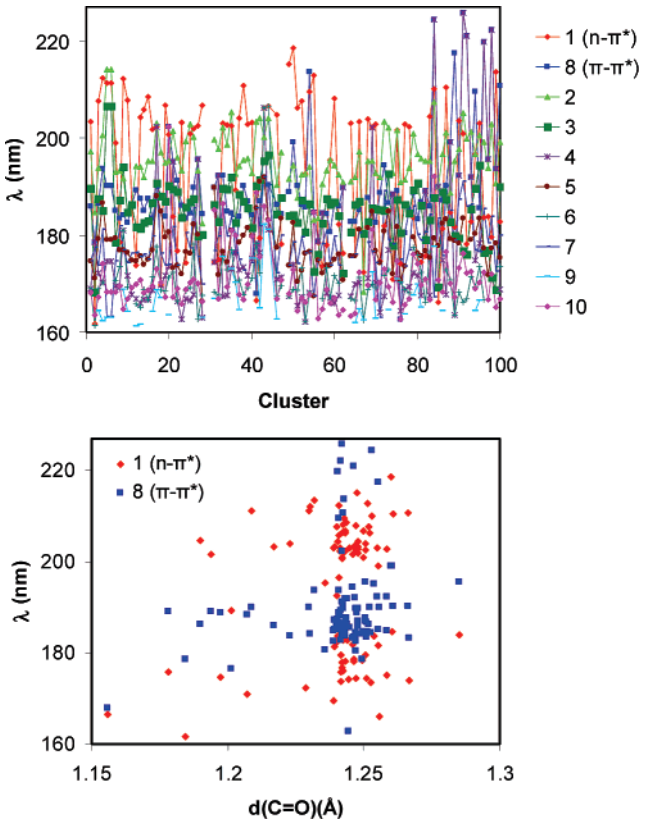

Figure 8. Top: Transition wavelength variations for 100 AA^-/water clusters calculated at the B3LYP/6-311++G**(6-31G)/CPCM approximation level. Bottom: Wavelength dependence on the C=O bond length in the same cluster set.

absorption intensities within the 190−200 nm range measured on the conventional spectrometer might not be as reliable as the rest of the spectra because of instrumental limitations. The experimental CD of the positively charged cation is very distinct from the signals of the two other forms, having opposite signs in both the lowest- and highest-wavelength regions.

Overall, the cluster computation does reproduce the main changes, albeit not in every single detail. The TD DFT method seems to underestimate the transitions' wavelengths. For example, the experimental absorption threshold observed at ∼210−215 nm is predicted at ∼195−205 nm. The error can be attributed not only to the inherent inaccuracy of the B3LYP model, but also to the continuum model approximation (see Table 3) that perhaps overestimates the influence of the bulk solvent. The positively charged form starts to absorb light in the lowest-wavelength region, which is correctly reproduced by the simulation. The difference in absorption between the negative and neutral forms is difficult to judge because the corresponding experiments have not been completed and the oscillations in the simulated absorption spectra do not appear to be realistic.

The CD spectra clearly provide more relevant information about the molecular structure than do the absorption spectra. Experimentally, very close matches are obtained for CD profiles of the zwitterions and the anion (AA^-), with a minimum at ∼196 nm and a maximum at ∼177 nm. The cation (AA^+) spectrum is clearly different, with a positive signal centered at ∼210 nm and a negative lobe at 187 nm. The simulation faithfully reproduces the AA^+ CD features, with a maximum at 208 nm and a minimum at 182 nm. The negative signal at the lowest wavelengths (below 170 nm), indicated by the measurement with the shorter path length (dashed line), is reproduced by the simulation. The computation also reproduces well the lower CD intensity of the anion compared to the zwitterion at the maximum of 177 nm (simulated at 178 nm). Within the range 200−160 nm, however, the simulation yields significantly greater differences between the AA^- and AAZW forms than the experimental data. Particularly, a weak positive signal is predicted for AA^- at 212 nm that does not have an experimental counterpart. We explain this inconsistency in part by the inadequate MD force field and complex conformational behavior of the AA^- form. There might also be a weak positive experimental signal at ∼223 nm for the zwitterions, not reflected in the simulation. However, the simulation correctly predicts the anion longest-wavelength CD to be more negative than that of the zwitterion.

Calculated and experimental absolute absorption intensities cannot be compared quantitatively because of the limited instrument range and solvent interference. Simulated CD absolute intensities ($\Delta\epsilon$) are overestimated by approximately a factor of 2 on average. This can still be considered as a very good result, given the volatility to the functional (cf. Figure 6) and solvent model (Figure 7). The volatility is also increased because of the intensity dependence on the square (or product) of the transition momenta.[71] The accuracy is comparable to that of similar studies.[20] The overestimation contrasts with vibrational circular dichroism, where comparable simulations provided only about 20−30% of the observed intensities.[72]

Geometry, Basis Set, and Solvent Variations. This and other studies[22,27,34−36] have indicated a significant role for environmental factors in the formation of the electronic spectral shapes of peptides. The role of the position of solvent molecules is represented, for example, in Figure 10, where absorption and CD spectra are simulated for three randomly selected AAZW/water clusters (out of the total of 100 giving the average shape in Figure 9). Clearly, according to the number and position of the solvent molecules, the spectral intensities exhibit large variations. This dependence implies the need for averaging of a relatively high number of MD configurations to obtain converged and realistic absorption and CD patterns. As discussed previously[27,36] and as is apparent from the orbital changes (Figures 2−5), the direct participation of the water electronic structure in the solute transition is the main factor responsible for the band frequency and intensity dispersion, apart from the pure electrostatic influence.

Obviously, once the environment is given, the spectral shapes directly reflect the conformations of the peptide. We analyzed this dependence for the two conformers of AA^- (Table 1) that have similar energies. The absorption and CD spectra obtained by the cluster averaging are given in Figure 11 for both forms. Upon comparison with the experimental spectra (Figure 9), we can conclude that the second conformer (2) provides more realistic CD profiles than the first one (1), in both low- and high-wavelength regions. Differences in absorption spectra do not appear significant at the current level of computational and experimental accuracy. Because the second conformer also appeared to be favored energetically, the simulations are thus consistent with the fact that this conformer represents the dominant population in the sample. Nevertheless, we noticed that the split negative signal in the range 200−250 nm computed for AA^- (2) was not observed experimentally. To explain this difference, we propose that, apart from possible conformer equilibrium and TD DFT error, the rotation of the NH_2 and CO_2^- groups might play a role as well. As indicated above, the rotation of the NH_2 group is particularly strongly coupled with

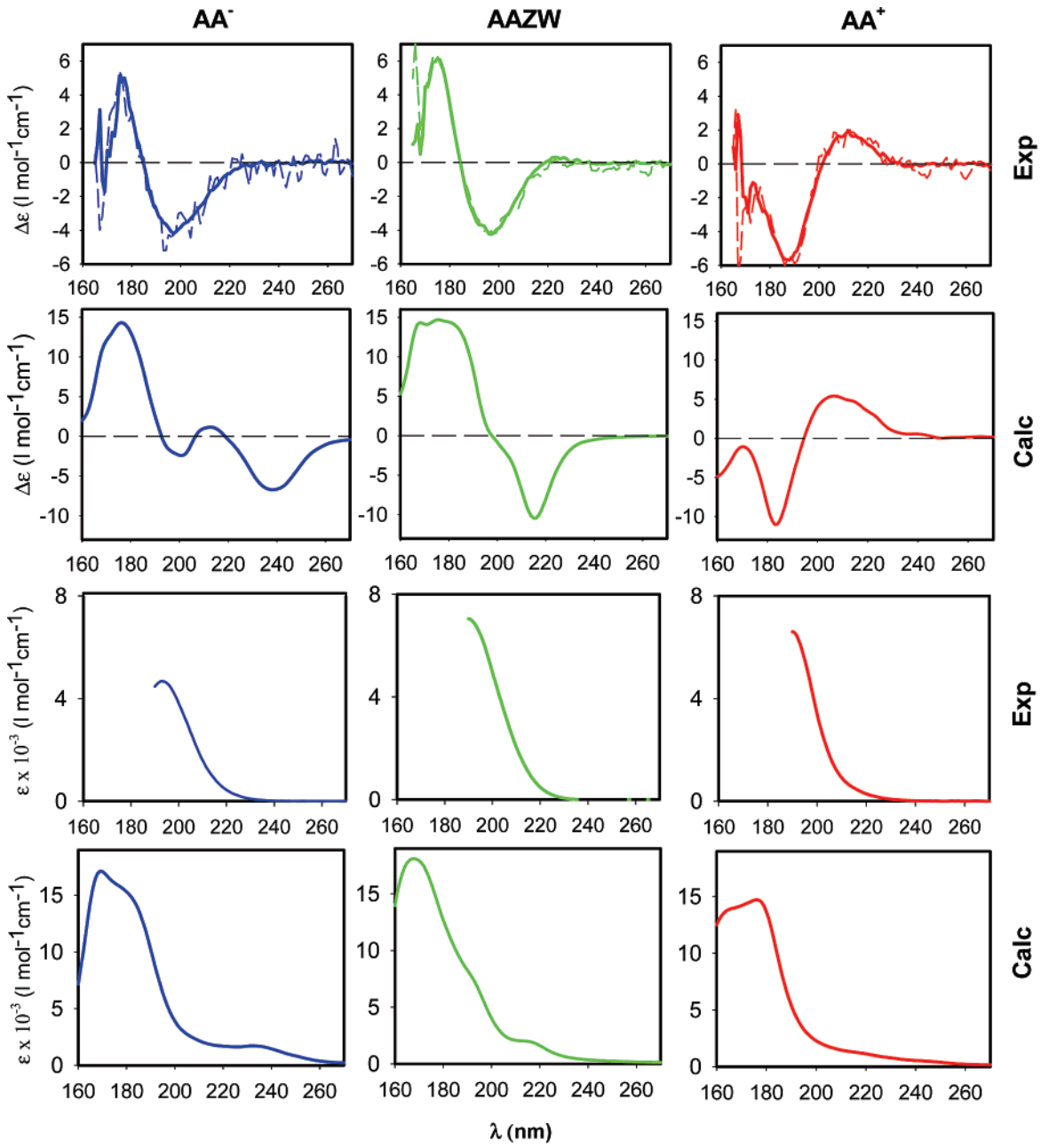

Figure 9. Experimental and simulated CD and absorption spectra of AA^+ (red), AAZW (green), and AA^-(blue). In the experimental data, the red, green, and blue lines correspond to AA solutions of pH 1.43, 6.17, and 12.1, respectively; the CD was measured with 18- and 6-μm cells (solid and dashed curves, respectively), and the absorption was measured with a 200-μm cell.

the main-chain dipeptide movement, and the detailed hydrogen-bonding pattern might not be correctly reproduced with the continuum or MD models.

The influence of rotation of the polar groups on ECD spectra has also been observed for the alanine zwitterion.[38] A somewhat analogous situation was also found in proline and alanine ORD[73] and proline and alanine zwitterion Raman and Raman optical activity (ROA),[49,74] where movements of charged groups dramatically affect the spectra. This multidimensional problem cannot be investigated in full for AA, because of computer limitations. Nevertheless, the role of the NH_2 and CO_2^- dynamics in the shaping of the spectra can be estimated in the lower two panels of Figure 11 where, for both of the AA^- main-chain conformations (1′, 2′), the H−N−C−O and O═C−C−N torsion angles were fixed in the MD cluster generation according to the BPW91/CPCM/6-311++G** equilibrium values. Clearly, even this seemingly small change induces considerable alterations in the CD spectral shapes and might explain the occurrence of the negative minimum at 196 nm.

We suspect that the ab initio PCM model underestimates the hydrogen-bond strengths of the polar groups with the solvent. The explicit solvent MD modeling might not be reliable in this respect because of its empirical character. However, variations of PCM model parameters do not lead to dramatic changes. At least the three models (CPCM/UA0, CPCM/UFF, IEF PCM) provided as Gaussian options compared for an AA^-/water cluster in Figure 12 provide essentially the same spectra. The cavity size does not seem to affect the spectral region of interest, and participating orbitals seem to be mostly confined within the default cavity space (Figure 4s in the SI). Because of the averaging over many clusters, even the detailed hydrogen-bonding pattern does not seem to correlate directly with the

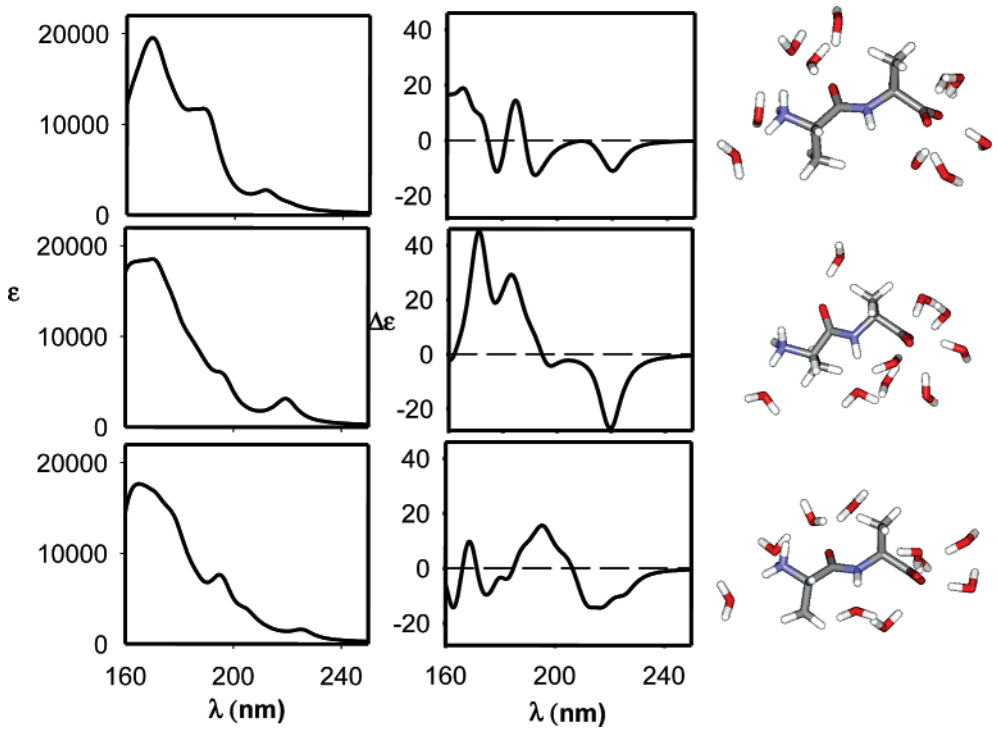

Figure 10. Absorption (left) and CD (right) spectra calculated (B3LYP/CPCM/6-311++G**) for three randomly selected AAZW/water clusters.

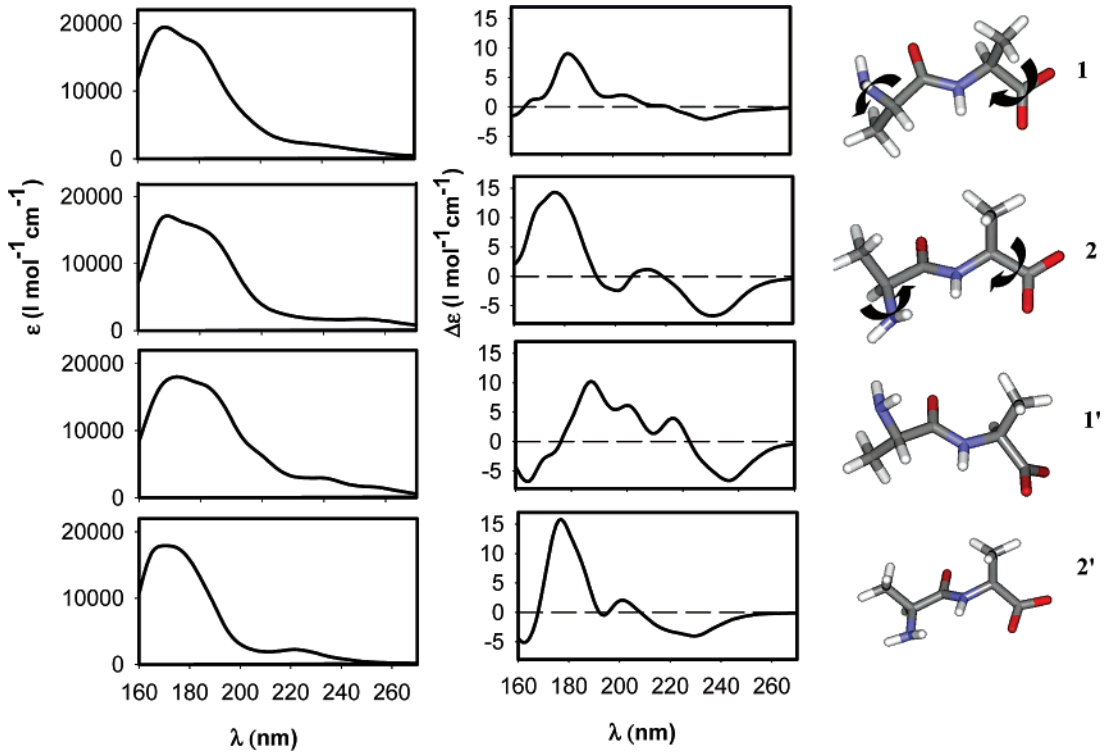

Figure 11. Cluster average absorption (left) and CD (right) spectra calculated for the four AA^- conformational models detailed in Tables 1 and 2 [conformers 1 and 2, with free (1, 2) and constrained (1′, 2′) NH_2 and CO_2^- rotations].

resultant spectral shape. For example, AA^- clusters with one and two hydrogen bonds to the carboxyl group (Figure 5s, SI) provide rather similar spectral shapes. Nevertheless, because of the discrepancies between implicit and explicit solvent modeling (cf. Figure 7), current efforts to develop more generalized solvent models still appear quite desirable.[36]

The mixed 6-311++G**(6-31G) basis set might certainly become a limited factor for higher-frequency transitions. We have already seen that the virtual orbitals are more affected than the occupied ones (Figure 2s, SI). However, trial computations with the full 6-311++G** basis (Figure 6s in the SI) indicate that the basis limit is not decisive for obtaining a converged spectral pattern for the amide group. On the other hand, we recall that the inclusion of the diffuse function (++) appeared necessary.[27] This brings us to the conclusion that the mixing of the water and amide electron structures is real and not induced by a basis set superposition error. Consequently, simplified QM/MM approaches not comprising explicit solvent

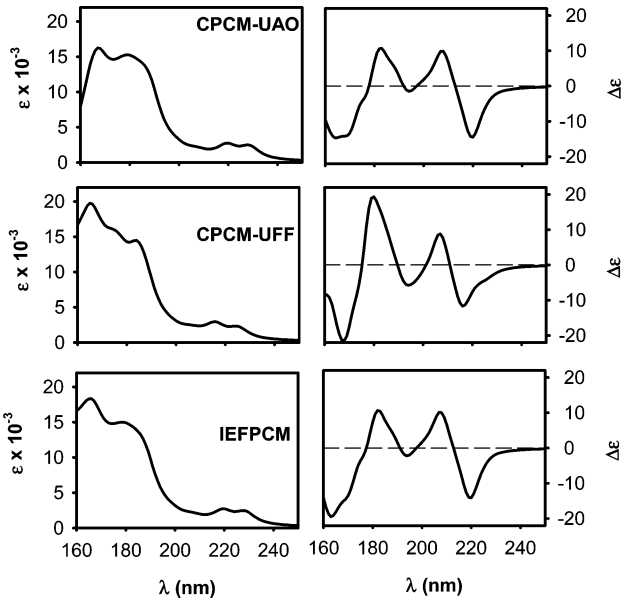

Figure 12. Calculated [B3LYP/6-311++G**(6-31G)] absorption (left) and CD (right) spectra for an arbitrarily selected AA^-/water cluster with three solvent models (CPCM/UA0, CPCM/UFF, and IEFPCM).

molecules are not suitable for modeling of the electric phenomena.

Conclusions

By employing the synchrotron radiation circular dichroism technique, we were able to acquire the spectra of various dialanine forms in a wider wavelength range than would have been possible by common instruments. This enabled us to obtain richer information about the molecular structure hidden in the spectral shapes. Most experimental features observed in the three AA forms could be reproduced by computations based on combined MD/QM modeling. The experimental CD shape of the cationic form was very different from that of the other two. The analysis nevertheless revealed that this difference was not directly linked to the backbone conformation. The CD shapes were significantly affected by interactions with water molecules. The solute orbital structure was significantly modulated by hydrogen-bonded solvent in particular. The present study thus indicates that such factors should be taken into account in future CD conformational studies of peptides and proteins, although such quantum solvent treatment requires considerable computer power.

Acknowledgment. This work was supported by the Grant Agency of the Czech Republic (Grant 203/06/0420), the Grant Agency of the Academy of Sciences (Grant A400550702), Grant OTKA NI61786, and the European Union Research Infrastructure Action FP6 (Integrated Activity on Synchrotron and Free Electron Laser Science, Contract RII3-CT-2004-506008). We thank Dr. Radek Pelc for the help with the manuscript.

Supporting Information Available: Additional figures documenting computational details and trial comparisons. This material is available free of charge via the Internet at http://pubs.acs.org.

References and Notes

(1) Johnson, W. C. *Methods Biochem. Anal.* **1985**, *31*, 61.
(2) Wallce, B. A. *J. Synchrotron Radiat.* **2000**, *7*, 289.
(3) Bose, P. K.; Polavarapu, P. L. *Carbohydr. Res.* **1999**, *319*, 172.
(4) Bose, P. K.; Polavarapu, P. L. *J. Am. Chem. Soc.* **1999**, *121*, 6094.
(5) Beychok, S. Circular dichroism of poly-α-amino acids and proteins. In *Poly-α-amino Acids: Protein Models for Conformational Analysis*; Fasman, G. D., Ed.; Marcel Dekker: New York, 1967; p 293.
(6) Greenfield, N.; Fasman, G. D. *Biochemistry* **1969**, *8*, 4108.
(7) Pančoška, P. Circular dichroism in analysis of biomolecules. In *Encyclopedia of Analytical Chemistry*; Meyers, R. A., Ed.; John Wiley & Sons Ltd.: Chichester, U.K., 2000; p 244.
(8) Johnson, W. C. *Proteins* **1999**, *35*, 307.
(9) Johnson, W. C., Jr. Electronic circular dichroism spectroscopy of nucleic acids. In *Landolt Bornstein Numerical Data and Functional Relationships in Science and Technology*; Saenger, W., Ed.; Springer-Verlag: Berlin, 1990; Vol. 1, p 1.
(10) *Circular Dichroism Principles and Applications*; Berova, N., Nakanishi, K., Woody, R. W., Eds.; Wiley-VCH: New York, 2000.
(11) Pančoška, P.; Frič, I.; Bláha, K. *Collect. Czech. Chem. Commun.* **1979**, *44*, 1296.
(12) Keiderling, T. A.; Wang, B.; Urbanová, M.; Pančoška, P.; Dukor, R. K. *Faraday Discuss.* **1994**, *99*, 263.
(13) Rogers, D. M.; Hirst, D. M. *Biochemistry* **2004**, *43*, 11092.
(14) Woody, R. W.; Sreerama, N. *J. Chem. Phys.* **1999**, *111*, 2844.
(15) Sreerama, N.; Woody, R. W. Circular dichroism of peptides and proteins. In *Circular Dichroism Principles and Applications*; Nakanishi, K., Berova, N., Woody, R. W., Eds.; Wiley-VCH: New York, 2000; p 601.
(16) Bartolotti, L. J.; Flurchick, K. An introduction to density functional theory. In *Reviews in Computational Chemistry*; Lipkowitz, K. B., Boyd, D. B., Eds.; VCH Publishers: New York, 1996; Vol. 7; p 187.
(17) Furche, F.; Ahlrichs, R. *J. Chem. Phys.* **2002**, *116*, 7433.
(18) Bak, K. L.; Hansen, A. E.; Ruud, K.; Helgaker, T.; Olsen, J.; Jørgensen, P. *Theor. Chim. Acta* **1995**, *90*, 441.
(19) Dierksen, M.; Grimme, S. *J. Phys. Chem. A* **2004**, *108*, 10225.
(20) Osted, A.; Kongsted, J.; Mikkelsen, K. V.; Christiansen, O. *Chem. Phys. Lett.* **2006**, *429*, 430.
(21) McCann, D. M.; Stephens, P. J. *J. Org. Chem.* **2006**, *71*, 6074.
(22) Pecul, M.; Marchesan, D.; Ruud, K. *J. Chem. Phys.* **2005**, *122*, 024106.
(23) Pecul, M.; Ruud, K.; Helgaker, T. *Chem. Phys. Lett.* **2004**, *388*, 110.
(24) Hirst, J. D.; Colella, K.; Gilbert, A. T. B. *J. Phys. Chem. B* **2003**, *107*, 11813.
(25) Rogers, D. M.; Hirst, J. D. *Chirality* **2004**, *16*, 234.
(26) Bouř, P. *J. Phys. Chem. A* **1999**, *103*, 5099.
(27) Šebek, J.; Kejík, Z.; Bouř, P. *J. Phys. Chem. A* **2006**, *110*, 4702.
(28) Rogers, D. M.; Besley, N. A.; O'Shea, P.; Hirst, J. D. *J. Phys. Chem. B* **2005**, *109*, 23061.
(29) Gilbert, A. T. B.; Hirst, J. D. *J. Mol. Struct. (THEOCHEM)* **2004**, *675*, 53.
(30) Hirst, J. D.; Hirst, D. M.; Brooks, C. L. *J. Phys. Chem. A* **1997**, *101*, 4821.
(31) Hagarman, A.; Measey, T.; Doddasomayajula, R. S.; Dragomir, I.; Eker, F.; Griebenow, K.; Schweitzer-Stenner, R. *J. Phys. Chem. B* **2006**, *110*, 6979.
(32) Krimm, S. Vibrational spectroscopy of polypeptides. In *Modern Polymer Spectroscopy*; Zerbi, G., Ed.; Wiley-VCH: New York, 1999; p 239.
(33) Bouř, P.; Keiderling, T. A. *J. Phys. Chem. B* **2005**, *109*, 23687.
(34) Besley, N. A. *Chem. Phys. Lett.* **2004**, *390*, 124.
(35) Cammi, R.; Corni, S.; Mennucci, B.; Tomasi, J. *J. Chem. Phys.* **2005**, *122*, 104513.
(36) Mennucci, B.; Martínez, J. M. *J. Phys. Chem. B* **2005**, *109*, 9818.
(37) Valiev, M.; Kowalski, K. *J. Chem. Phys.* **2006**, *125*, 211101.
(38) Fukuyama, T.; Matsuo, K.; Gekko, K. *J. Phys. Chem. A* **2005**, *109*, 6928.
(39) Caricato, M.; Mennucci, B.; Tomasi, J.; Ingrosso, F.; Cammi, R.; Corni, S.; Scalmani, G. *J. Chem. Phys.* **2006**, *124*, 124520.
(40) Messer, B. M.; Cappa, C. D.; Smith, J. D.; Wilson, K. R.; Gilles, M. K.; Cohen, R. C.; Saykally, R. J. *J. Phys. Chem. B* **2005**, *109*, 5375.
(41) Dragomir, I. C.; Measey, T. J.; Hagarman, A. M.; Schweitzer-Stenner, R. *J. Phys. Chem. B* **2006**, *110*, 13235.
(42) Eker, F.; Griebenow, K.; Schweitzer-Stenner, R. *J. Am. Chem. Soc.* **2003**, *125*, 8178.
(43) Lucas, B.; Gregoire, H.; Maitre, P.; Ortega, J. M.; Rupenyan, A.; Reimann, B.; Scherman, J. P.; Desfrancois, C. *Phys. Chem. Chem. Phys.* **2004**, *6*, 2659.
(44) Diem, M.; Lee, O.; Roberts, G. M. *J. Phys. Chem.* **1992**, *96*, 548.
(45) Knapp-Mohammady, M.; Jalkanen, K. J.; Nardi, F.; Wade, R. C.; Suhai, S. *Chem. Phys.* **1999**, *240*, 63.
(46) Weir, A. F.; Lowrey, A. H.; Williams, R. W. *Biopolymers* **2001**, *58*, 577.
(47) Zuk, W. M.; Freedman, T. B.; Nafie, L. A. *Biopolymers* **1989**, *28*, 2025.
(48) Jalkanen, K. J.; Nieminen, R. M.; Knapp-Mohammady, M.; Suhai, S. *Int. J. Quantum Chem.* **2003**, *92*, 239.

(49) Kapitán, J.; Baumruk, V.; Kopecký, V., Jr.; Bouř, P. *J. Phys. Chem. A* **2006**, *110*, 4689.
(50) Bouř, P.; Kapitán, J.; Baumruk, V. *J. Phys. Chem. A* **2001**, *105*, 6362.
(51) Dreuw, A.; Head-Gordon, M. *J. Am. Chem. Soc.* **2004**, *126*, 4007.
(52) Tozer, D. J. *J. Chem. Phys.* **2003**, *119*, 12697.
(53) Guennic, B. L.; Hieringer, W.; Görling, A.; Autschbach, J. *J. Phys. Chem. A* **2005**, *109*, 4836.
(54) Bouř, P.; Buděšínský, M.; Špirko, V.; Kapitán, J.; Šebestík, J.; Sychrovský, V. *J. Am. Chem. Soc.* **2005**, *127*, 17079.
(55) Limao-Vieira, P.; Giuliani, A.; Delwiche, J.; Parafita, R.; Mota, R.; Duflot, D.; Flament, J. P.; Drage, E.; Cahillane, P.; Mason, N. J.; Hoffmann, S. V.; Hubin-Franskin, M. J. *Chem. Phys.* **2006**, *324*, 339.
(56) Becke, A. *Phys. Rev. A* **1988**, *38*, 3098−3100.
(57) Frisch, M. J.; Trucks, G. W.; Schlegel, H. B.; Scuseria, G. E.; Robb, M. A.; Cheeseman, J. R.; Montgomery, J. A., Jr.; Vreven, J. T.; Kudin, K. N.; Burant, J. C.; Millam, J. M.; Iyengar, S. S.; Tomasi, J.; Barone, V.; Mennucci, B.; Cossi, M.; Scalmani, G.; Rega, N.; Petersson, G. A.; Nakatsuji, H.; Hada, M.; Ehara, M.; Toyota, K.; Fukuda, R.; Hasegawa, J.; Ishida, M.; Nakajima, T.; Honda, Y.; Kitao, O.; Nakai, H.; Klene, M.; Li, X.; Knox, J. E.; Hratchian, H. P.; Cross, J. B.; Adamo, C.; Jaramillo, J.; Gomperts, R.; Stratmann, R. E.; Yazyev, O.; Austin, A. J.; Cammi, R.; Pomelli, C.; Ochterski, J. W.; Ayala, P. Y.; Morokuma, K.; Voth, G. A.; Salvador, P.; Dannenberg, J. J.; Zakrzewski, V. G.; Dapprich, S.; Daniels, A. D.; Strain, M. C.; Farkas, O.; Malick, D. K.; Rabuck, A. D.; Raghavachari, K.; Foresman, J. B.; Ortiz, J. V.; Cui, Q.; Baboul, A. G.; Clifford, S.; Cioslowski, J.; Stefanov, B. B.; Liu, G.; Liashenko, A.; Piskorz, P.; Komaromi, I.; Martin, R. L.; Fox, D. J.; Keith, T.; Al-Laham, M. A.; Peng, C. Y.; Nanayakkara, A.; Challacombe, M.; Gill, P. M. W.; Johnson, B.; Chen, W.; Wong, M. W.; Gonzalez, C.; Pople, J. A. *Gaussian 03, Revision C.02*; Gaussian Inc.: Pittsburgh, PA, 2003.
(58) Klamt, A.; Schuurmann, G. *J. Chem. Soc., Perkin Trans.* **1993**, *2*, 799.
(59) Barone, V.; Cossi, M.; Tomasi, J. *J. Comput. Chem.* **1998**, *19*, 404.
(60) Lee, C.; Yang, W.; Parr, R. G. *Phys. Rev. B* **1988**, *37*, 785.
(61) Hamprecht, F. A.; Cohen, A. J.; Tozer, D. J.; Handy, N. C. *J. Chem. Phys.* **1998**, *109*, 6264.
(62) Ponder, J. W. *TINKER—Software Tools for Molecular Design*, version 3.8; Washington University School of Medicine: Saint Louis, MO, 2000.
(63) Pearlman, D. A.; Case, D. A.; Caldwell, J. W.; Ross, W. S.; Cheatham, T. E.; Debolt, S.; Ferguson, D. M.; Seibel, G.; Kollman, P. A. *Comput. Phys. Commun.* **1995**, *91*, 1.
(64) Jorgensen, W. L.; Chandrasekhar, J.; Madura, J. D. *J. Chem. Phys.* **1983**, *79*, 926.
(65) Bouř, P.; Michalík, D.; Kapitán, J. *J. Chem. Phys.* **2005**, *122*, 144501.
(66) Zhao, Y.; Truhlar, D. G. *J. Phys. Chem. A* **2006**, *110*, 13126.
(67) Becke, A. D. *J. Chem. Phys.* **1993**, *98*, 1372.
(68) Becke, A. D. *J. Chem. Phys.* **1993**, *98*, 5648.
(69) Perdew, J. P.; Wang, Y. *Phys. Rev. B* **1992**, *45*, 13244.
(70) Boese, A. D.; Doltsinis, N. L.; Handy, N. C.; Sprik, M. *J. Chem. Phys.* **2000**, *112*, 1670.
(71) Bouř, P. *Chem. Phys. Lett.* **2002**, *365*, 82.
(72) Bouř, P.; McCann, J.; Wieser, H. *J. Phys. Chem. A* **1998**, *102*, 102.
(73) Pecul, M.; Ruud, K.; Rizzo, A.; Helgaker, T. *J. Phys. Chem. A* **2004**, *108*, 4269.
(74) Kapitán, J.; Baumruk, V.; Kopecký, V., Jr.; Pohl, R.; Bouř, P. *J. Am. Chem. Soc.* **2006**, *128*, 13451.